Traveling waves and chaos in thermosolutal convection

A. E. Deane
Joint Institute for Laboratory Astrophysics, National Bureau of Standards and University of Colorado, Boulder, Colorado 80309-0440 and Department of Astrophysical, Planetary, and Atmospheric Sciences, University of Colorado, Boulder, Colorado 80309-0391

E. Knobloch
Department of Physics, University of California, Berkeley, California 94720

J. Toomre*
Joint Institute for Laboratory Astrophysics, National Bureau of Standards and University of Colorado, Boulder, Colorado 80309-0440 and Department of Astrophysical, Planetary, and Atmospheric Sciences, University of Colorado, Boulder, Colorado 80309-0391

(Received 10 March 1987)

Numerical experiments on two-dimensional thermosolutal convection reveal oscillations in the form of traveling, standing, modulated, and chaotic waves. Transitions between these wave forms and steady convection are investigated and compared with theory. Such rich nonlinear behavior is possible in fluid layers of wide horizontal extent, and provides an explanation for waves observed in recent laboratory experiments with binary fluid mixtures.

I. INTRODUCTION

Nonlinear dynamical systems can exhibit a wide variety of oscillations, with periodic motion often replaced by aperiodic or chaotic motion through a succession of transitions as the forcing is increased. The nature of these transitions has been of growing interest in a variety of disciplines. Recently attention has focused on continuous systems, described by partial differential equations, as part of a general program to elucidate the processes that lead to pattern formation in physical systems.

The present paper is a contribution to the study of pattern formation arising from a Hopf bifurcation in a continuous translationally invariant system. Such a bifurcation gives rise to various types of wave motion. Doubly diffusive systems, such as thermosolutal convection[1–6] and convection in binary mixtures,[7–11] provide a relatively simple example within which the competition between different waveforms in the nonlinear regime may be investigated. Although our study of thermosolutal convection is restricted to two dimensions, we are able to show that the oscillations can develop variously into traveling, standing, modulated, and chaotic waves. Traveling waves in which a pattern of rolls drifts to the left or right with a uniform speed (which depends on the rate of heating from below) are the preferred form into which an oscillatory instability develops for a wide range of parameters. Transitions between the different wave states and steady convection are investigated; similar transitions have been found in recent experiments on binary fluid mixtures in which traveling waves have been observed.[8–10]

In contrast to our earlier study[3,6] of the transition to chaos of oscillations in the form of standing waves, the work described here uses periodic boundary conditions in the horizontal to model a fluid layer of large aspect ratio. This allows us to relate the existence of the traveling and modulated waves to the resulting change in the symmetry properties of the partial differential equations.

II. THERMOSOLUTAL SYSTEM

Thermosolutal convection is characterized by the competition between the destabilizing effect of heating a fluid layer from below and the stabilizing effect of maintaining a solute concentration which increases with depth. The driving and restoring buoyancy forces are shifted in phase because the solute diffuses less rapidly than heat. If the solute gradient is sufficiently strong, convection can set in through a Hopf bifurcation even when the mean density decreases upward.

Thermosolutal convection in two dimensions is described by the nondimensionalized equations[1,6]

$$\sigma^{-1}[\partial_t \nabla^2 \Psi + J(\Psi, \nabla^2 \Psi)] = R_T T_x - R_S S_x + \nabla^4 \Psi \ , \tag{1a}$$

$$\partial_t T + J(\Psi, T) = \nabla^2 T \ , \tag{1b}$$

$$\partial_t S + J(\Psi, S) = \tau \nabla^2 S \ , \tag{1c}$$

with x and z the horizontal and vertical coordinates and t the time. Here Ψ is the stream function, T and S are the temperature and solute concentrations, and $J(f,g) \equiv f_x g_z - f_z g_x$. The parameters R_T and R_S are the thermal and solutal Rayleigh numbers, and are a measure of the forcing of the system by the temperature and solute gradients imposed across the fluid layer; σ is the Prandtl number, and τ $(0 < \tau < 1)$ is the ratio of the solutal to the thermal diffusivity.

The fluid is confined between horizontal stress-free boundaries held at fixed temperatures and solute concentrations, with the lower boundary hotter and saltier than

the upper boundary. The boundary conditions on the horizontal surfaces are

$$\Psi=\Psi_{zz}=0, \quad T=S=1, \quad z=0 , \tag{2a}$$

$$\Psi=\Psi_{zz}=0, \quad T=S=0, \quad z=1 . \tag{2b}$$

Periodic conditions in the horizontal require $\Psi(0,z,t)=\Psi(l,z,t)$, where l is the spatial period, and likewise for T and S. The problem is thus specified by the five dimensionless parameters R_T, R_S, τ, σ and l, along with the boundary and initial conditions.

The system possesses two types of basic solutions, traveling waves (TW) and standing waves (SW), both of which bifurcate simultaneously from the conduction solution when the thermal Rayleigh number reaches[1]

$$R_T^{(o)}=\left[1+(1+\sigma+\tau)\frac{\tau}{\sigma}\right]R_0+\left[\frac{\sigma+\tau}{\sigma+1}\right]R_S , \tag{3}$$

where R_0 is the critical Rayleigh number for the onset of Rayleigh-Bénard convection.

The SW solution branch was investigated previously[2,3,6] with impenetrable and insulating boundary conditions on $x=0,l$, thereby eliminating the TW solution branch. However, when traveling waves are admitted by the boundary conditions, we reported[12] that both numerical experiments and theory show that near the Hopf bifurcation at $R_T^{(o)}$ standing waves are unstable with respect to traveling wave disturbances for a wide range of parameter values. Here we explore the properties of traveling waves in considerable detail, and in addition show that modulated and chaotic waves can be realized in such a double-diffusive system.

III. SMALL-AMPLITUDE THEORY

The solutions for R_T near $R_T^{(o)}$ are described by amplitude equations of the form[12-15]

$$\dot{A}_l=(\lambda+a A_r^2+b A^2+c A_r^4+d A^2 A_r^2+e A^4)A_l+\mathcal{O}(7) , \tag{4a}$$

$$\dot{A}_r=(\lambda+a A_l^2+b A^2+c A_l^4+d A^2 A_l^2+e A^4)A_r+\mathcal{O}(7) , \tag{4b}$$

$$\dot{\phi}_l=\omega+\alpha A_r^2+\beta A^2+\gamma A_r^4+\delta A^2 A_r^2+\epsilon A^4+\mathcal{O}(6) , \tag{4c}$$

$$\dot{\phi}_r=\omega+\alpha A_l^2+\beta A^2+\gamma A_l^4+\delta A^2 A_l^2+\epsilon A^4+\mathcal{O}(6) , \tag{4d}$$

with the dot denoting time derivatives, and $\mathcal{O}(n)$ terms of order n. Here $A_l, A_r(>0)$ are amplitudes of left- and right-traveling waves and ϕ_l,ϕ_r are the corresponding phases, in terms of which

$$\Psi(x,z,t)=\mathrm{Re}[A_l(t)e^{i[kx+\phi_l(t)]}+A_r(t)e^{i[kx-\phi_r(t)]}]\times\sin\pi z+\mathcal{O}(3) . \tag{5}$$

The higher-order terms involve spatial harmonics whose coefficients can be expressed in terms of A_l and A_r. Expansions similar to (5) apply for T and S. The quantity λ is the bifurcation parameter, proportional to $R_T-R_T^{(o)}$, and $\omega-\Omega=\mathcal{O}(\lambda)$, where Ω is the frequency of the neutrally stable oscillations[2-5] at $\lambda=0$ ($\Omega^2>0$). The total amplitude $A^2\equiv A_l^2+A_r^2$ is proportional to the amplitude of the Nusselt number, N_T, measuring the heat transport. The coefficients of the nonlinear terms in (4) are real, independent of λ near $\lambda=0$, and can be computed[13,14] from Eqs. (1). One finds that $b=0$ (Refs. 12 and 13). In Fig. 1 we show the coefficients a,e as functions of R_S for $\tau=10^{-1/2}$, $\sigma=1$, and $l=3$. Observe that a can change sign, while e is always negative. When a is small but nonzero various secondary bifurcations also occur at small amplitude, i.e., in the regime of validity of Eqs. (4). We make use of this fact to determine the various nonlinear solutions of Eqs. (4) and the possible transitions among them.

When the nonlinear terms in (4) are deleted, one recovers the results describing the linear stability of the conduction solution. To determine the stationary solutions we set $\dot{A}_l=\dot{A}_r=0$, and solve the resulting Eqs. (4a) and (4b) for (A_l,A_r). There are five solutions: the conduction solution (0,0), a left-traveling wave $(A_l,0)$, a right-traveling wave $(0,A_r)$, a standing wave $(A/\sqrt{2},A/\sqrt{2})$, and a mixed mode (A_l,A_r) with $A_l\neq A_r$. Since the two frequencies $\dot{\phi}_l,\dot{\phi}_r$ are distinct when $A_l\neq A_r$, we call the mixed mode a modulated wave (MW). The stability of each of these solutions is determined by linearizing Eqs. (4a) and (4b) about the solutions and computing the two eigenvalues. The results for the case $d>0>c>-d$ are summarized in Fig. 2, showing A^2 as a function of λ for each of the four solutions in the (a,e) plane. We do not distinguish between left- and right-traveling waves. The signs $-$ and $+$ denote stable and unstable eigenvalues. The first is a total-amplitude eigenvalue, and changes sign at saddle-node bifurcations. The second eigenvalue determines the relative stability of TW and SW and vanishes at secondary bifurcations producing MW. Observe that provided $a\neq 0$, SW can never be stable near onset, and that if $a<0$ and e is sufficiently negative, a nonhysteretic transition from a stable TW branch to a stable SW branch occurs via a stable MW branch. If $c(d+c)>0$ a tertiary Hopf bifurcation from the MW branch can occur, producing a quasi-periodic wave with three frequencies.[15,16] This

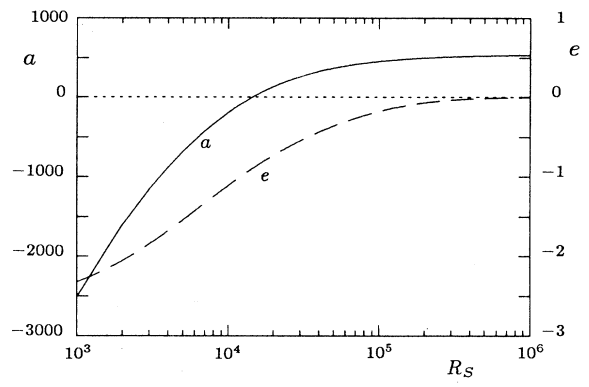

FIG. 1. Coefficients a and e in Eqs. (4) evaluated as functions of R_S for $\tau=10^{-1/2}$, $\sigma=1$, and $l=3$. Note that a changes sign at $R_S=14\,585.4$, while e is always negative.

possibility is not shown in Fig. 2. As $|a|$ increases, the secondary and tertiary bifurcations and the MW branch move to $\mathcal{O}(1)$ amplitudes and out of the regime of validity of the analysis, and one recovers the results of Ref. 12. However, the fact that the solutions discovered by this local analysis persist at large amplitude even for values of a far from $a=0$ is invaluable in interpreting the numerical results described below.

The interaction between the TW, SW branches and the branch of steady-state convection (SS) can be studied in the neighborhood of $R_T=R_T^{(c)}$, $R_S=R_S^{(c)}$ at which the conduction solution has a double-zero eigenvalue.[17] The dynamics of the system is now described by a complex amplitude $B(t)$ in terms of which $\Psi(x,z,t)=\mathrm{Re}\{Be^{ikx}\}\sin(\pi z)+\mathcal{O}(3)$, satisfying the equation[14,18]

$$\ddot{B}=(u+\eta|B|^2-|B|^4)B + \nu\dot{B}+\tfrac{1}{2}a(\bar{B}\dot{B}+B\dot{\bar{B}})B+e|B|^4\dot{B}\ . \quad (6)$$

Here μ, ν are linearly related to $R_T-R_T^{(c)}$, $R_S-R_S^{(c)}$; a, e, and $\eta\equiv-\frac{1}{2}\Omega(\alpha+\beta)$ are evaluated in the limit $R_T\to R_T^{(c)}$, $R_S\to R_S^{(c)}$. Thus a,e are both negative. In (6) we have included two essential fifth-order terms to make the TW branch nondegenerate and to get the SS branch to turn towards larger R_T. If we write $B=re^{i\phi}$, then the five solution types of interest are pure conduction ($r=0$), SS ($\dot{r}=0,\dot{\phi}=0$), TW ($\dot{r}=0,\dot{\phi}\neq0$), SW ($\dot{r}\neq0,\dot{\phi}=0$), and MW ($\dot{r}\neq0,\dot{\phi}\neq0$). The TW branch always terminates on the SS branch in a steady-state bifurcation. In Fig. 3 we exhibit bifurcation diagrams describing two scenarios of interest to the present problem. In Fig. 3(a), the TW branch terminates on the unstable subcritical SS branch, and the transition to the stable SS branch is hysteretic. In some cases the TW branch may lose stability at a secondary Hopf bifurcation to MW (not shown). Figure 3(b) shows a nonhysteretic transition between stable TW and stable SS branches. Again, we expect that away from $R_T^{(c)}$, $R_S^{(c)}$ the basic features of the transition between TW and SS predicted by (6) remain unchanged. Thus the transition can be hysteretic as in Fig. 3(a), with the stability of the upper SS branch unaffected by TW, or nonhysteretic as in Fig. 3(b) where the SS branch gains stability at the bifurcation. In either case the phase speed of the traveling waves vanishes as $c_p\propto(R_T-R_T^{(TW)})$ near the end point $R_T=R_T^{(TW)}$ (see Fig. 3).

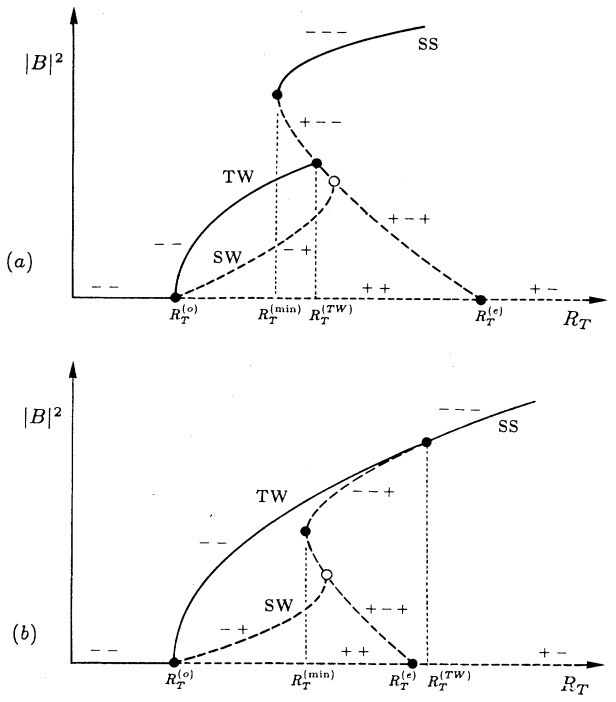

FIG. 3. Bifurcation diagrams from Eq. (6) showing the transition from traveling waves (TW) and standing waves (SW) to steady convection (SS) for (a) $a,e<0,\ 0<\eta=\mathcal{O}(1)$; and (b) $a,e<0,\ 0<\eta\ll1$. Stable solutions are indicated by solid lines. Solid circles indicate local bifurcations, open ones global bifurcations. The third eigenvalue on the SS branch describes stability with respect to traveling-wave perturbations.

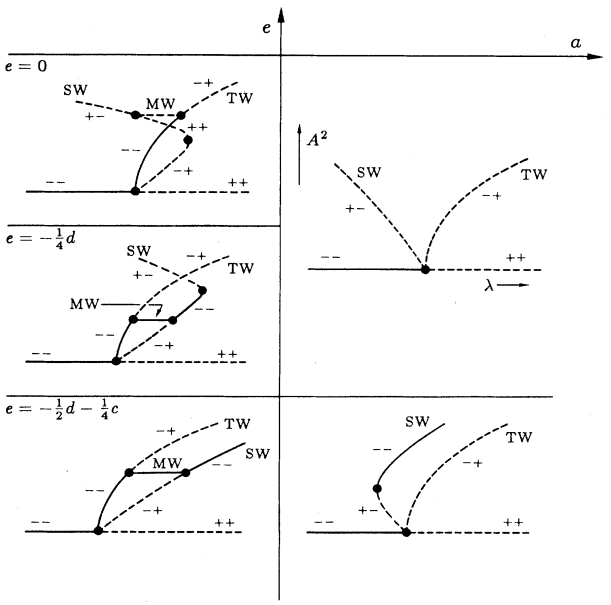

FIG. 2. Bifurcation diagrams (A^2 vs λ) in the (a,e) plane, as obtained from Eqs. (4) for $|a|\ll1$, $d>0>c>-d$, showing transitions between the traveling wave (TW) and standing wave (SW) branches via a modulated wave (MW) branch. Solid lines indicate stable solutions.

IV. NUMERICAL SOLUTIONS

We have used finite-difference techniques[6,19] to numerically integrate the full partial differential equations (1) subject to the boundary conditions (2). The nonlinear numerical code specifies Ψ, $\nabla^2\Psi$, T and S on grids staggered in space and time; the difference scheme has second-order accuracy and is centered in both space and time. Within a time step the nonlinear terms are treated explicitly and the diffusive terms are represented by a DuFort-Frankel scheme. The associated Poisson equation linking the

stream function Ψ and vorticity $\nabla^2\Psi$ is solved by Fourier decomposition and tridiagonal elimination. The spatial representation typically employs 16 mesh points in the vertical and 48 points in the horizontal when $l=3$. This value of l is chosen to be close to $2^{3/2}$, the wavelength of the instability. The first solutions were started from a no-motion state while imposing small-amplitude random perturbations on the thermal and solutal fields. Subsequent solutions were obtained usually by employing solutions nearby in parameter space as initial conditions. We have checked the results by using two different codes which yield nearly identical results.

We have surveyed the behavior of solutions by varying the parameter R_T for three different values of R_S, considering (i) $R_S=10^4$, (ii) $R_S=14\,585.4$, and (iii) $R_S=10^5$, while taking $\tau=10^{-1/2}$, $\sigma=1$, $l=3$. For such parameters the SW branch bifurcates supercritically in (i) ($a<0$), vertically in (ii) ($a\simeq 0$), and subcritically in (iii) ($a>0$); the TW branch always bifurcates vertically. We have numerically obtained solutions in the form of TW, SW, MW as well as chaotic waves (CW) and SS, and studied the transitions between them as a function of R_T.

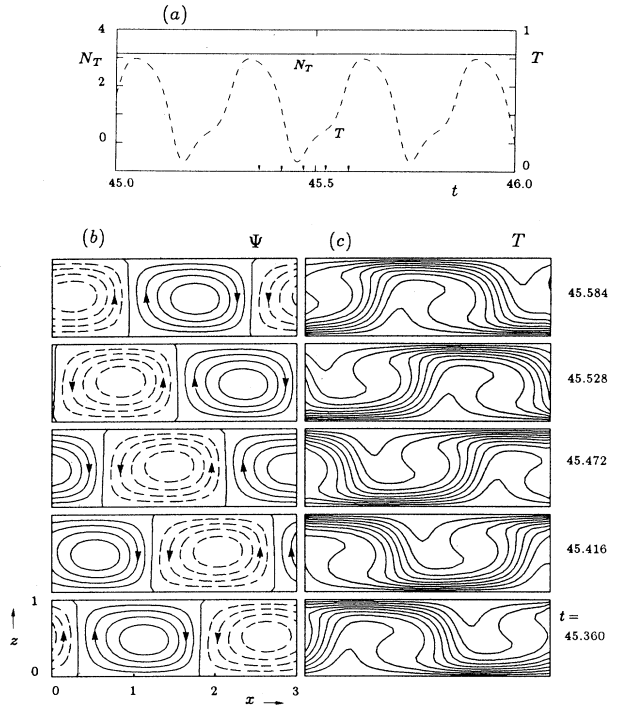

FIG. 4. Traveling-wave (TW) solution of the partial differential equations for $R_T=14\,000$ from survey (ii). In (a), time histories of the thermal Nusselt number at the mid-depth, $N_T(\frac{1}{2}, t)$, and temperature as sampled at a fixed point, $T(\frac{3}{4}, \frac{3}{4}, t)$. Time, t, is in units of the thermal diffusion time across the layer. Shown in (b) are contour plots of the stream-function field Ψ over the computational domain (x,z) for the successive times as indicated. The contour intervals for Ψ are 0.2; the circulation sense is indicated. In this TW the pattern travels to the left at constant speed $c_p=10.5$. Shown in (c) are the corresponding contour plots of the temperature field T, revealing the presence of tilted thermal plumes.

A. Traveling and standing waves

Figure 4 shows the stream function and temperature fields at successive times for a traveling wave when $R_T=14\,000$ in (ii). At any given instant in time the pattern consists of two convective rolls with the indicated senses of circulation. The pattern drifts to the left with a constant phase speed c_p. If viewed at a given spatial point the flow appears to oscillate with a frequency $\omega_0=c_p k$, where $k=2\pi/l$, as the pattern sweeps past it [see Fig. 4(a)]. In a frame moving to the left with speed c_p the motion is steady, and hence horizontally averaged quantities like the thermal and solutal Nusselt numbers N_T and N_S, or the kinetic energy E, are independent of time.

In contrast, Fig. 5 presents the stream function and temperature fields for a standing wave at successive times when $R_T=10\,800$ in (ii). In such a wave the sense of the flow reverses cyclically with frequency ω_0, but the two rolls making up the convection cell do not translate in x. In contrast to a traveling wave, N_T, N_S, and E in the standing wave oscillate with frequency $2\omega_0$. The solution shown has temporal symmetry, with the transport by the clockwise and anticlockwise motions being similar [see Fig. 5(a)]. In our calculations we have found that a SW computed with impenetrable sidewalls[2,3,5,6] typically develops into a TW when the horizontal boundary conditions are changed to periodic ones,[12] in agreement with the small-amplitude theory. If a solution is started from

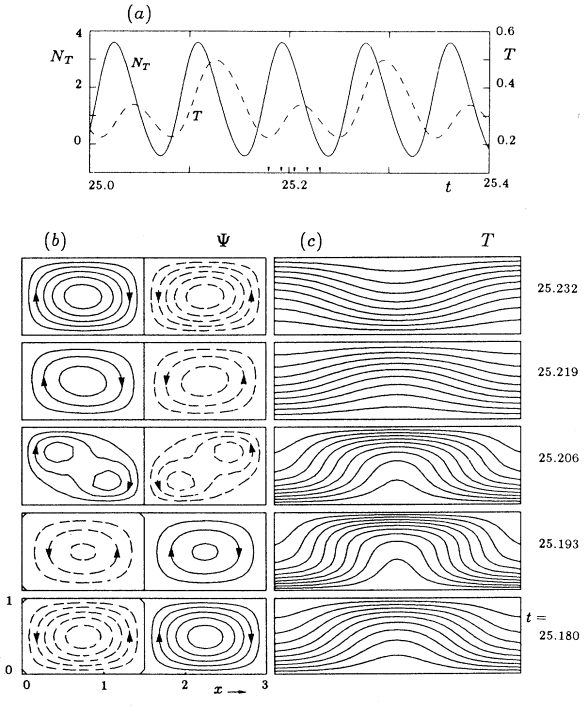

FIG. 5. As in Fig. 4, but for a standing-wave (SW) solution at successive times for $R_T=10\,800$ from survey (ii). The time spanned corresponds to a little less than one-half period. The contours of Ψ are at intervals of 0.1, except for the nearly quiescent middle frame where the intervals are reduced to 0.01. The sense of circulation is seen to reverse cyclically, producing both upward and downward directed thermal plumes.

small random perturbations to a quiescent state, the transient behavior may be quite complicated, involving rolls that are variously modulated in amplitude and that translate. The asymptotic approach to the final SW or TW states can be slow, and the evolution probably reflects the presence of all the competing, albeit unstable, solution branches.

The numerical solutions reveal important differences between the spatial structure of a SW and a TW. In a SW [Fig. 5(c)] the thermal and solutal plumes are symmetrically positioned about the centers of the ascending and descending columns of fluid. But in a TW [Fig. 4(c)] the plumes are asymmetrical about the cell centers, and have a characteristic tilt from the vertical. As a consequence, within a SW the production of vorticity by the buoyancy forces, which serves to modulate and change the sense of the circulation within each roll, proceeds symmetrically about the center of the cells. But in a TW the vorticity production proceeds largely in the tilted plumes, and these are displaced laterally from the principal vorticity within each roll. One finds that negative vorticity is produced to one side of the region of positive vorticity within one roll, while positive vorticity is produced on the same side of the region of negative vorticity within the other roll. Such erosion of vorticity in the rolls leads to a translation of the overall pattern, thereby yielding a TW.

Figure 6 shows bifurcation sequences as a function of R_T in (i), (ii), and (iii), using E as a measure of A^2. Figure 6(a) presents results for (i). The conduction solution loses stability at a Hopf bifurcation when R_T reaches $R_T^{(o)}=7725$, and gives rise to a branch of stable traveling waves (see Fig. 4). As R_T increases, E increases monotonically, while the oscillation frequency ω_0 (not shown) decreases monotonically from its bifurcation value of 31.4 (in units of radians per thermal diffusion time), reaching zero at $R_T \simeq 14\,000$. At this point c_p vanishes and the wave turns into steady-state convection. This transition is a steady-state bifurcation and stability is transferred to the SS branch for larger R_T with no hysteresis. It is possible to follow the SS branch to smaller values of R_T by imposing impenetrable boundary conditions to eliminate TW. The calculation shows that with periodic boundary conditions this part of the SS branch is unstable with respect to TW, but is stable with respect to SW in the interval $R_T^{(\min)} \leq R_T \lesssim 14\,000$. Here $R_T^{(\min)}$ is the smallest value of R_T at which SS convection exists, and corresponds to a saddle-node bifurcation on the SS branch.[3,4] These results are entirely consistent with the small amplitude theory summarized in Fig. 3.

Figure 6(b) shows results for (ii). The Hopf bifurcation occurs at $R_T^{(o)}=10\,743$, and both TW and SW branches bifurcate vertically. At larger R_T stable standing waves are found. The resulting oscillations are indicated in Fig. 6(b) as vertical lines through the mean value, representing the range of values taken by E during one period. The vigor of the motion increases with R_T, until at $R_T \simeq 11\,250$ the SW branch loses stability to traveling waves. The TW branch can be followed down to at least $R_T \simeq 11\,100$ before it loses stability to standing waves again. The traveling waves have lower kinetic energy than the mean value for the standing waves at the same R_T. According to the theory summarized in Fig. 2, transitions between SW and TW branches can only occur via a secondary MW branch. Since the observed transition is hysteretic the MW branch must be unstable, and we conjecture that the bifurcation diagram is as shown in Fig. 7. This diagram is readily obtained from Eqs. (4) by taking $a=b=0$, and including seventh-order terms in the analysis. However, both the presence of the MW branch and its stability depend on these terms. These, like the coefficients c and d, have not been calculated.

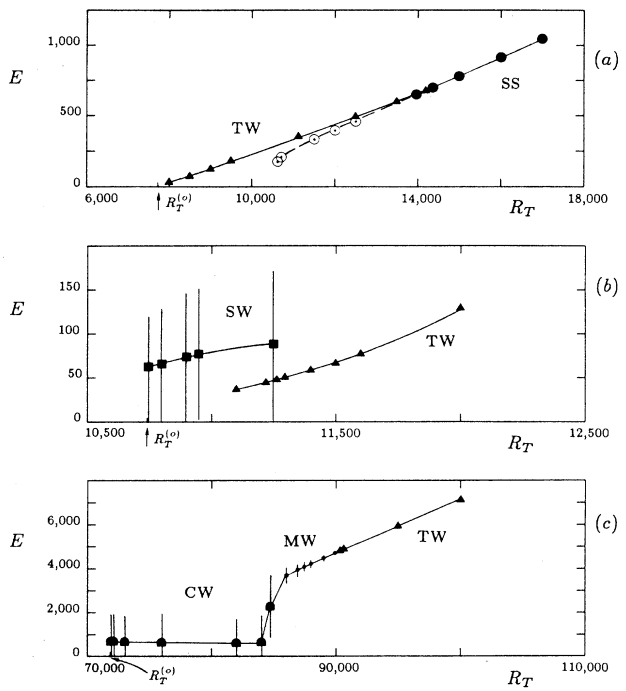

FIG. 6. Bifurcation sequences showing the variation of the kinetic energy E with R_T as determined from sequences of numerical solutions of the partial differential equations for (a) $R_S = 10^4$ [survey (i)]; (b) $R_S = 14\,585.4$ (ii); and (c) $R_S = 10^5$ (iii). Distinctive symbols identify solutions as traveling waves (TW), standing waves (SW), modulated waves (MW), and chaotic waves (CW). Open circles denote the unstable part of the steady-state (SS) solution branch in (a). Vertical lines indicate typical range of E within the time-varying solutions in (b) and (c).

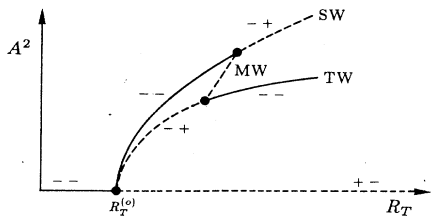

FIG. 7. A possible bifurcation diagram when $a=b=0$, and $e<0, d+c>0, d+\frac{1}{2}c>0, e+\frac{1}{2}d+\frac{1}{4}c<0$, showing a hysteretic transition between SW and TW branches.

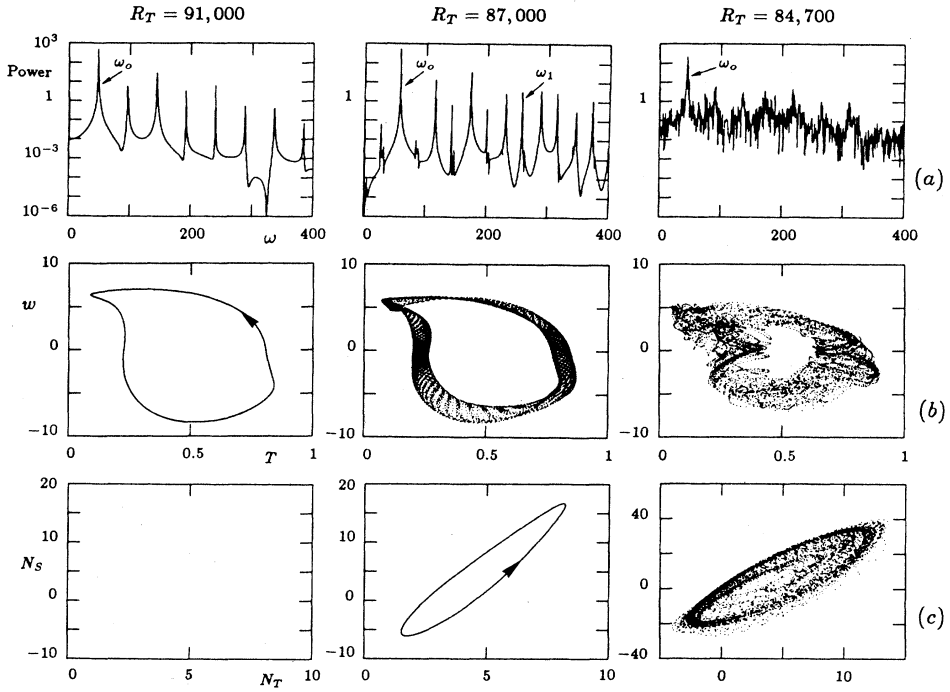

FIG. 8. Three numerical solutions from survey (iii) ($R_S = 10^5$) at indicated values of R_T. Shown in (a) are power spectra of $T(\frac{3}{4},\frac{3}{4},t)$ with frequency ω, in (b) phase projections of $w(\frac{3}{4},\frac{3}{4},t)$ vs $T(\frac{3}{4},\frac{3}{3},t)$ and in (c) orbits of $N_T(\frac{1}{2},t)$ vs $N_S(\frac{1}{2},t)$.

B. Modulated waves and chaos

Figure 6(c) presents results for (iii), revealing bifurcations that lead to chaos. To clarify the behavior, three solutions from this sequence in R_T are shown in the composite Fig. 8, presenting for each the power spectrum of the temperature T as sampled at a point in the flow, the projection of the trajectory in phase space onto a plane with that T and the corresponding vertical velocity w as coordinates, and the projection onto the $N_T - N_S$ plane. This is a reverse sequence and we describe it as R_T is decreased from a large value. At $R_T = 100\,000$ there are traveling waves of the type described earlier. As R_T is decreased, we find as expected that N_T, N_S, and E decrease while c_p increases. Figure 8(a) shows that at $R_T = 91\,000$ there is a traveling wave; the power spectrum of the temperature is seen to consist only of the frequency ω_0 associated with the pattern translation and its harmonics. For this R_T, Fig. 8(b) shows that w and T describe a 1-torus; Fig. 8(c) indicates that N_T and N_S are constant, appearing as a single point.

As R_T is decreased further, at $R_T = 90\,000$ there appears a rapid modulation in the amplitude of the traveling waves, signaling the appearance of modulated waves (MW). This modulation increases as R_T is decreased such that at $R_T = 87\,000$ a second frequency ω_1 is clearly visible in the spectrum [Fig. 8(a)]; ω_1 is large (= 262.0) and is apparently incommensurate with $\omega_0 = 48.4$. All the other frequencies in the spectrum are identifiable as $n\omega_0 \pm m\omega_1$, with $n, m = 0, 1, 2, \ldots$. The power spectra of N_T, N_S, and E (not shown) reveal only the presence of the frequency ω_1 and its harmonics. For this R_T, Fig. 8(b) shows the 2-torus on which w and T lie, and Fig. 8(c) the 1-torus on which N_T and N_S lie.

As R_T is decreased even further, the modulation grows as indicated in Fig. 6(c), until at $R_T = 84\,900$ there appear chaotic modulations to the traveling waves. We denote such solutions as chaotic waves (CW). We have verified that the chaotic behavior persists when the spatial resolution is doubled. For $R_T = 84\,700$, Fig. 8(a) shows that the solution has a temperature spectrum consisting of peaks at ω_0 and its harmonics and a generally noisy background, indicating chaos. The motion here consists of two rolls, traveling roughly with speed c_p and with random or chaotic modulations of the amplitudes. Figures 8(b) and 8(c) show that the smooth tori have now been replaced by "fuzzy" tori. For $R_T \lesssim 84\,000$ the waves have ceased to travel, and the chaotic state can be followed to $R_T = 71\,830$, very close to $R_T^{(o)} = 71\,829.5$.

V. DISCUSSION AND CONCLUSIONS

The numerical solutions of the partial differential equations describing thermosolutal convection have shown that traveling, standing, modulated, and chaotic waves are readily found for suitably chosen parameter values. In particular, stable SW are found only near parameter values for which the coefficient a in (4) vanishes. The three different parameter values were chosen to describe phenomena characteristic of the three possibilities (i) $a < 0$, (ii) $a \simeq 0$, (iii) $a > 0$. In (i), the TW branch is stable, and terminates in a steady-state bifurcation on the SS branch, with c_p vanishing linearly as the distance from the bifurcation. At the steady-state bifurcation stability is ex-

changed between the TW and SS branches with no hysteresis. In (ii), both SW and TW can coexist, and the observed hysteretic transition between them is conjectured to occur via an unstable MW branch. In (iii), chaotic waves are observed near the turning point on the TW branch. We have not investigated the origin of these solutions, but note that in a horizontally unbounded system, the onset of chaos cannot occur via a Hopf bifurcation on the TW branch followed by frequency locking and a cascade of period doubling bifurcations—the translational invariance prevents frequency locking.[20] In this respect we expect qualitative differences between unbounded and bounded systems. In addition, the possibility remains that the chaotic waves are a manifestation of wavelength increasing instabilities that are prohibited by the imposed spatial periodicity.[21]

The system studied here is not readily amenable to laboratory experiments because of the difficulties in constructing horizontal boundaries that permit a flux of solute, in addition to that of heat, through them. However, in binary-fluid mixtures characterized by a negative Soret coefficient, a stabilizing concentration gradient is set up in response to a destabilizing temperature gradient. Then the solute distribution is controlled by the applied temperature difference across the layer according to $R_S = -\psi R_T$, where ψ ($\psi < 0$) is the separation ratio and is proportional to the Soret coefficient. Thus the interesting dynamics found in both systems owes its existence to the competition between a destabilizing temperature gradient and a stabilizing concentration distribution. For this reason the equations describing binary-fluid mixtures are closely related to Eqs. (1).[22] Consequently, one may draw from the present study a number of qualitative conclusions about the binary-fluid mixtures.

Both the theory and numerical calculations[12] show that, with periodic boundary conditions, the Nusselt number N_T produced by traveling waves is constant in time. The same will be true for binary-fluid mixtures, and experiments on a water-ethanol mixture[9] show that when the number of rolls is even, N_T exhibits no detectable oscillations even though the container is of finite extent. We also expect that, for appropriate parameter values, binary mixtures will exhibit the type of transitions between traveling waves and steady convection described in the present paper. Specifically, a transition similar to that shown in Fig. 3(a) may have been observed in normal ^{3}He-^{4}He bulk mixture[11] if the constant N_T states found near the Hopf bifurcation are identified with traveling waves instead of steady convection.[23] A transition of the form shown in Fig. 3(b) has been observed in a water-ethanol mixture,[9] although the experiments reveal some evidence for hysteresis near the TW-SS transition that apparently arises from three-dimensional phenomena not described by Eqs. (1). In addition, the phase velocity of the traveling waves vanishes linearly as the transition is approached,[9] as predicted theoretically.[14] In that experiment the traveling waves are identified unambiguously using shadowgraph visualization. Finally, in a recent experiment[10] a bifurcation from finite-amplitude traveling waves to modulated waves has also been observed. The properties of the transition are consistent with the theoretical predictions[18,24] based entirely on the translation and reflection symmetries of these systems.

As already mentioned, the coefficient b in the amplitude equations (4) vanishes for the boundary conditions (2). The same is true for binary mixtures with the corresponding boundary conditions.[13] Consequently, the bifurcation to TW is degenerate, and SW are unstable near the onset of instability even when they bifurcate supercritically.[12] In the present paper we have shown that stable SW can be found but only for parameter values close to those for which the coefficient a also vanishes. More specific predictions await the calculation of the coefficients a and b in Eqs. (4) for the experimental parameter values and boundary conditions. We anticipate, however, that b will be positive but small, so that TW will bifurcate subcritically as revealed by the experiments,[8,9,11] but acquire stability at a secondary saddle-node bifurcation. This would explain why the oscillatory instability does not equilibrate at small amplitudes near onset.[8,9] However, in contrast to our numerical results, in the experiments an initial disturbance develops for $R_T > R_T^{(o)}$ directly into a growing TW transient with negligible amplitude oscillations. Overall, with $b > 0$ Figs. 3(a) and 3(b) provide a consistent summary of the experimental results.

In this paper we have not attempted to simulate the experiments on binary-fluid mixtures. Instead we have employed local bifurcation analysis based on the translation and reflection invariance of a plane layer coupled with numerical simulations of a thermosolutal convective system to emphasize those results that are independent of the detailed equations, parameter values or boundary conditions. It is these features that we expect to be characteristic of not only binary-fluid mixtures, but also of other doubly diffusive systems such as magnetoconvection[25] or convection in a layer constrained by rotation.[26]

ACKNOWLEDGMENTS

We are indebted to D. R. Moore for advice and for the use of the numerical code that he developed for various applications. We thank N. O. Weiss for stimulating discussions. The work at Berkeley was supported by the Applied and Computational Mathematics Program of the U.S. Defense Advanced Research Projects Agency. The work at Colorado was supported by the U.S. National Aeronautics and Space Administration through Grants No. NAGW-91 and No. NSG-7511 and Contract No. NAS8-31958. The Joint Institute for Laboratory Astrophysics is supported jointly by the University of Colorado and the National Bureau of Standards.

*Also at Naval Ocean Research and Development Activity, National Space Technology Laboratories, NSTL, MS 39529.

[1]G. Veronis, J. Fluid Mech. **34**, 315 (1968).

[2]H. E. Huppert and D. R. Moore, J. Fluid Mech. **78**, 821 (1976).

[3]D. R. Moore, J. Toomre, E. Knobloch, and N. O. Weiss, Nature **303**, 663 (1983).

[4]L. N. Da Costa, E. Knobloch, and N. O. Weiss, J. Fluid Mech. **109**, 25 (1981).

[5]C. S. Bretherton and E. A. Spiegel, Phys. Lett. **96A**, 152 (1983).
[6]E. Knobloch, D. R. Moore, J. Toomre, and N. O. Weiss, J. Fluid Mech. **166**, 409 (1986).
[7]H. Brand, P. C. Hohenberg, and V. Steinberg, Phys. Rev. A **30**, 2548 (1984).
[8]R. W. Walden, P. Kolodner, A. Passner, and C. M. Surko, Phys. Rev. Lett. **55**, 496 (1985); P. Kolodner, A. Passner, C. M. Surko, and R. W. Walden, *ibid.* **56**, 2621 (1986).
[9]E. Moses and V. Steinberg, Phys. Rev. A **34**, 693 (1986).
[10]R. Heinrichs, G. Ahlers, and D. S. Cannell, Phys. Rev. A **35**, 2761 (1987); G. Ahlers, D. S. Cannell, and R. Heinrichs (unpublished).
[11]G. Ahlers and I. Rehberg, Phys. Rev. Lett. **56**, 1373 (1986).
[12]E. Knobloch, A. E. Deane, J. Toomre, and D. R. Moore, Contemp. Math. **56**, 203 (1986).
[13]E. Knobloch, in *Proceedings of the 1985 Joint ASCE-ASME Mechanics Conference,* edited by N. E. Bixler and E. A. Spiegel (Fluid Eng. Div., ASME, New York, 1985), Vol. 24, p. 17.
[14]E. Knobloch, Phys. Rev. A **34**, 1538 (1986).
[15]E. Knobloch, Contemp. Math. **56**, 193 (1986).
[16]A detailed classification of the degenerate Hopf bifurcation with $\mathcal{O}(2)$ symmetry through topological codimension 3 has been given by M. Golubitsky and M. Roberts (unpublished); and J. D. Crawford and E. Knobloch (unpublished). These papers discuss the case when both a and b are small but nonzero.
[17]E. Knobloch, and M. R. E. Proctor, J. Fluid Mech. **108**, 291 (1981).
[18]G. Dangelmayr, and E. Knobloch, Philos. Trans. R. Soc. (to be published).
[19]D. R. Moore, R. S. Peckover, and N. O. Weiss, Comp. Phys. Commun. **6**, 198 (1974).
[20]D. Rand, Arch. Rat. Mech. Anal. **79**, 1 (1982).
[21]See, for example, H. T. Moon, P. Huerre, and L. G. Redekopp, Phys. Rev. Lett. **49**, 458 (1982); L. R. Keefe, Stud. Appl. Math. **73**, 91 (1985).
[22]E. Knobloch, Phys. Fluids **23**, 1918 (1980).
[23]E. Knobloch, A. E. Deane, and J. Toomre, in *The Physics of Structure Formation: Theory and Simulation,* edited by W. Güttinger and G. Dangelmayr (Springer-Verlag, Heidelberg, in press).
[24]E. Knobloch and J. B. Weiss, Phys. Rev. A (to be published).
[25]M. R. E. Proctor and N. O. Weiss, Rep. Prog. Phys. **45**, 1317 (1982); G. Dangelmayr and E. Knobloch, Phys. Lett. **117**, 394 (1986); E. Knobloch, Geophys. Astrophys. Fluid Dyn. **36**, 161 (1986).
[26]J. Guckenheimer and E. Knobloch, Geophys. Astrophys. Fluid Dyn. **23**, 247 (1983); J. M. Pfotenhauer, J. J. Niemela, and R. J. Donnelly, J. Fluid Mech. **175**, 85 (1987).